NASA/TM–20220014642

Low-Drag Acoustic Liner Development

Brian M. Howerton
Langley Research Center, Hampton, Virginia

Michael G. Jones
Langley Research Center, Hampton, Virginia

May 2023

NASA STI Program . . . in Profile

Since its founding, NASA has been dedicated to the advancement of aeronautics and space science. The NASA scientific and technical information (STI) program plays a key part in helping NASA maintain this important role.

The NASA STI program operates under the auspices of the Agency Chief Information Officer. It collects, organizes, provides for archiving, and disseminates NASA's STI. The NASA STI program provides access to the NTRS Registered and its public interface, the NASA Technical Reports Server, thus providing one of the largest collections of aeronautical and space science STI in the world. Results are published in both non-NASA channels and by NASA in the NASA STI Report Series, which includes the following report types:

- TECHNICAL PUBLICATION. Reports of completed research or a major significant phase of research that present the results of NASA Programs and include extensive data or theoretical analysis. Includes compilations of significant scientific and technical data and information deemed to be of continuing reference value. NASA counter-part of peer-reviewed formal professional papers but has less stringent limitations on manuscript length and extent of graphic presentations.

- TECHNICAL MEMORANDUM. Scientific and technical findings that are preliminary or of specialized interest, e.g., quick release reports, working papers, and bibliographies that contain minimal annotation. Does not contain extensive analysis.

- CONTRACTOR REPORT. Scientific and technical findings by NASA-sponsored contractors and grantees.

- CONFERENCE PUBLICATION. Collected papers from scientific and technical conferences, symposia, seminars, or other meetings sponsored or co-sponsored by NASA.

- SPECIAL PUBLICATION. Scientific, technical, or historical information from NASA programs, projects, and missions, often concerned with subjects having substantial public interest.

- TECHNICAL TRANSLATION. English-language translations of foreign scientific and technical material pertinent to NASA's mission.

Specialized services also include organizing and publishing research results, distributing specialized research announcements and feeds, providing information desk and personal search support, and enabling data exchange services.

For more information about the NASA STI program, see the following:

- Access the NASA STI program home page at http://www.sti.nasa.gov

- E-mail your question to help@sti.nasa.gov

- Phone the NASA STI Information Desk at 757-864-9658

- Write to:
  NASA STI Information Desk
  Mail Stop 148
  NASA Langley Research Center
  Hampton, VA 23681-2199

NASA/TM–20220014642

Low-Drag Acoustic Liner Development

Brian M. Howerton
Langley Research Center, Hampton, Virginia

Michael G. Jones
Langley Research Center, Hampton, Virginia

National Aeronautics and
Space Administration

Langley Research Center
Hampton, Virginia 23681-2199

May 2023

Available from:

NASA STI Program / Mail Stop 148
NASA Langley Research Center
Hampton, VA 23681-2199
Fax: 757-864-6500

This page intentionally left blank.

Table of contents page

List of Figures

List of Tables

Nomenclature and acronyms

a	duct width
b	duct height
c	speed of sound
d_h	duct hydraulic diameter
γ	ratio of specific heats
λ_{L+SW}	resistance factor of the liner plus the hardwall portion of the test section
λ_L	resistance factor of the liner
λ_{SW}	resistance factor of a smooth wall sample
L	length of perforation
LL	liner length
M	centerline flow Mach number
$p_{s\infty}$	static pressure, absolute
p	static pressure, differential
P_{atm}	atmospheric pressure
P	perimeter length of the test section
S	static pressure port separation distance
q	duct dynamic pressure
W	width of perforation
W_L	width of liner
x	streamwise duct coordinate
ρ	density

Executive summary

Interest in characterization of the aerodynamic drag of acoustic liners has increased in the past several years. This report details experiments in the NASA Langley Grazing Flow Impedance Tube to quantify the relative drag of several perforate-over-honeycomb liner configurations at flow speeds of M=0.3 and 0.5. Various perforate geometries and orientations are investigated to determine their resistance factors using a static pressure drop approach. Comparison of these resistance factors gives a relative measurement of liner drag. For these flow conditions, acoustic measurements are performed simultaneously with the drag measurements for tonal excitation from 400 to 3000 Hz at source sound pressure levels of 140 and 150 dB. Educed impedance and attenuation spectra are used to determine the impact of variations in perforate geometry on acoustic performance. The goal is to identify a perforate that will reduce the drag penalty associated with conventional round-hole perforates by 60%. One perforate design, based on a slot geometry, is shown to reduce this penalty by 50%. Further reductions may be possible but require a reduction in measurement uncertainty to allow a statistically rigorous evaluation.

I. INTRODUCTION

In the past, the aerodynamic drag due to acoustic liners in an aircraft engine nacelle was tolerated as a necessary penalty in order to achieve required noise levels. It is generally accepted that such liners increase drag relative to a smooth surface [1]. Research by Drouin has also shown that liner drag can be influenced by the ambient acoustic field [2]. Continued pressure on manufacturers to reduce engine emissions and fuel burn provides the motivation to understand and reduce drag associated with engine nacelle liners. Furthermore, new aircraft propulsion concepts such as the open-fan and configurations with distributed electric propulsion may lead to airframe designs where external liners (Figure 1) are required to meet community noise goals [3].

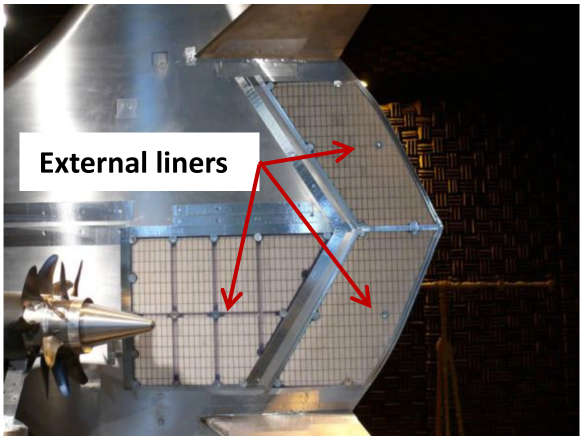

Figure 1. External liners on an Open-Rotor powered, Blended Wing-Body concept aircraft

NASA is committed to developing technologies that aggressively reduce aircraft fuel consumption and noise. To that end, creating a low-drag acoustic liner would be an important contribution. The majority of acoustic liners developed for production aircraft engines use a facesheet perforated with round holes to provide the necessary porosity for the liner to function. To study liner drag, Howerton and Jones [4] used an approach from Nikuradse [5] to calculate a resistance factor (λ) based on the static pressure drop within a lined duct. Using this approach, they demonstrated that reducing the perforate hole diameter reduced λ (and thus the drag) for a typical liner design (Figure 2). Note that the resistance factor for all perforates in Figure 2 was higher than for a hard wall (HW).

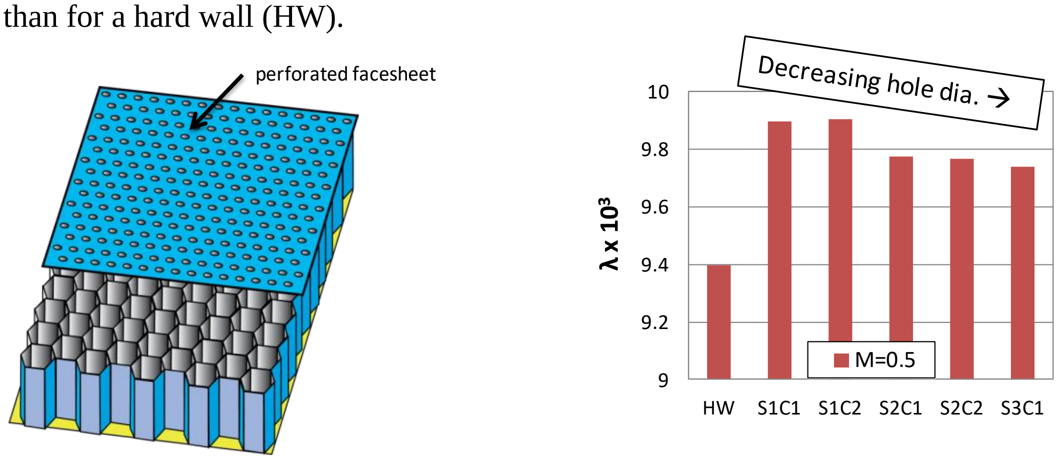

Figure 2. Conventional liner construction and the effect of perforate hole diameter on λ.

In addition to modifying the perforate hole diameter, changing the perforate geometry and orientation, relative to the flow, may create a configuration with improved drag performance. Advances in three-dimensional (3-D) printing allow for parametric studies of these concepts to develop an empirical database of geometric variations and are the first step towards formulation of analytical liner drag models.

The purpose of the current investigation is to evaluate the effects of perforate geometry and orientation on the drag for several novel facesheet perforate configurations. Each liner is tested in the NASA Langley Research Center Grazing Flow Impedance Tube, and the resultant acoustic and aerodynamic responses are compared to (1) determine which designs provide reduced drag, (2) determine the effects of the acoustic field on this drag, and (3) determine whether this drag reduction has an impact on the acoustic performance of the liner. Details are provided on the static pressure drop method used to compute λ along with a description of the liner samples tested. Later sections show these results for various perforate geometries with and without acoustic excitation. Data is also presented on liner acoustic performance focusing on the educed impedances and resulting attenuation.

II. LINER DRAG MEASUREMENTS

For this investigation, the drag of each configuration relative to a smooth wall will be determined by measuring differences in the static pressure drop along the duct wall opposite of the liner sample. This method can be applied to small ducts with fully developed, turbulent flow and is similar to Nikuradse's approach used for studying roughness in pipes [5]. With the static pressure data and selected flow parameters, one can compute the duct resistance factor, λ (also known as the 'friction factor'), given by the following:

$$\lambda = \frac{dp}{dx}\frac{d_h}{q} \tag{1}$$

using the hydraulic diameter of the flow duct for d_h:

$$d_h = \frac{2ab}{a+b} \tag{2}$$

and the compressible form for q:

$$q = \frac{\gamma}{2} p_\infty M^2 \tag{3}$$

The non-dimensional nature of λ allows the static pressure data to be normalized, taking out the run-to-run effects of slightly varying duct Mach number and static pressure. Note that λ encompasses the sum of both the skin friction and pressure components of drag. Thus, any effects of the liner cavity are also included, thereby differentiating this method from others that are solely measuring skin friction. The results of these calculations provide a relative measurement of drag between liner configurations.

III. EXPERIMENT

The experimental investigation involves testing eleven perforate facesheet-over-honeycomb liners and two smooth wall configurations in the GFIT. The facesheet samples are created using a 3-D printing process placed over a common liner core. An aluminum smooth wall sample (SW) and a 3-D printed resin smooth wall sample (RSW), each with no perforations, are included to provide reference baselines. For each configuration, a static pressure survey is performed along the length of the GFIT. Simultaneously, a measurement of the axial static pressure drop across the liner is made using higher accuracy instrumentation for computation of the liner resistance factor.

A. Facesheet Construction

The majority of the sheets designed for this experiment have a constant 8 percent open area (POA) and a sheet thickness of 0.762 mm. One sheet was built to a higher porosity of 14 POA while another was substantially thicker at 7.62 mm to give a thickness-to-hole diameter (T/D) ratio of 10 (in contrast to the typical value of ~1). Multiple perforate geometries are evaluated. In addition, a 3-D printed smooth wall sample (Resin SW) with no perforations is included to evaluate any inherent effects of the manufacturing process and material. Figure 3. Phase 1 Facesheet perforate geometry provides sketches of the test geometries for Phase 1. A summary of the key parameters for each perforation type is given in Table 1: Facesheet perforate dimensions.. Several round-hole perforates were constructed since this is the most common geometry in current use and is the simplest to manufacture. In addition to the Conventional sample with straight holes, variations in hole angle (45 and 60 deg from horizontal) and orientation are investigated. Orientations are defined as with (w), against (a) and perpendicular (p) to the flow direction. Note that setting orientation with or against the flow is achieved by rotating the angled-hole facesheets to reverse the leading and trailing edges. Alternate geometries of slots with the long axis both parallel and perpendicular to the flow, and diamond-shaped perforations are also considered. Based on data from a study by Hwang [6] which indicated that increasing the facesheet thickness may result in lower drag, a facesheet with a higher thickness-to-hole diameter (T/D) ratio of 10 was built as well. The facesheets were 3-D printed from photopolymer resin using a stereolithography (SLA) process with the flow surface sanded to ensure a smooth finish.

For Phase 2, several variations of slot geometries are studied based on the results from Phase 1 which showed drag reduction with the slot design. Details of the perforate shapes and dimensions are provided in Figure 4. The angled configurations are intended to induce a spanwise velocity to the flow while the two chevron perforates are an attempt to create longitudinal vorticity similar to the riblet low-drag treatments studied by various entities. Where applicable, some of the configurations are tested in the orientation as shown in Figure 4 and again in a reversed orientation to determine the effects of relative flow direction. A facesheet using the Perpendicular Slot previously constructed for Phase 1 is included for comparison.

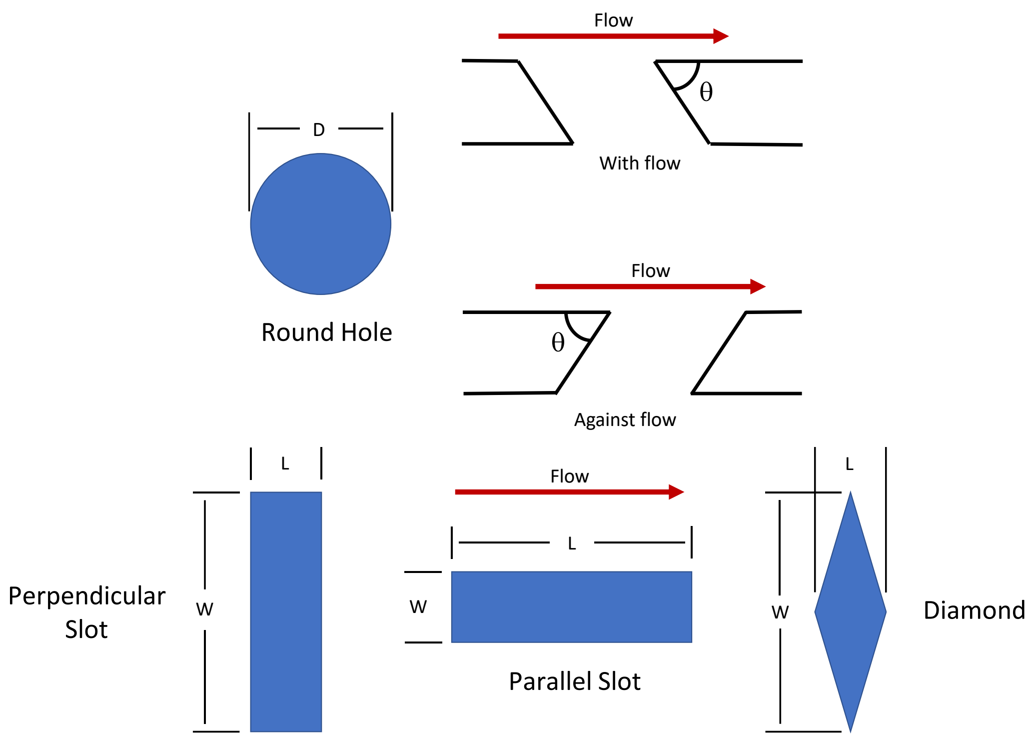

Figure 3. Phase 1 Facesheet perforate geometry.

Table 1: Facesheet perforate dimensions.

	Conventional	**60deg w/flow**	**60deg a/flow**	**45deg w/flow**	**45deg a/flow**	**60deg p/flow**	**High POA**	**High T/D**
D (mm)	0.762	0.762	0.762	0.762	0.762	0.762	1.016	0.762
θ (deg)	90	45	45	60	60	60	90	90

	Parallel Slot	**Perpendicular Slot**	**Diamond**
L (mm)	2.032	0.508	0.508
W (mm)	0.508	2.032	2.032
θ (deg)	90	90	90

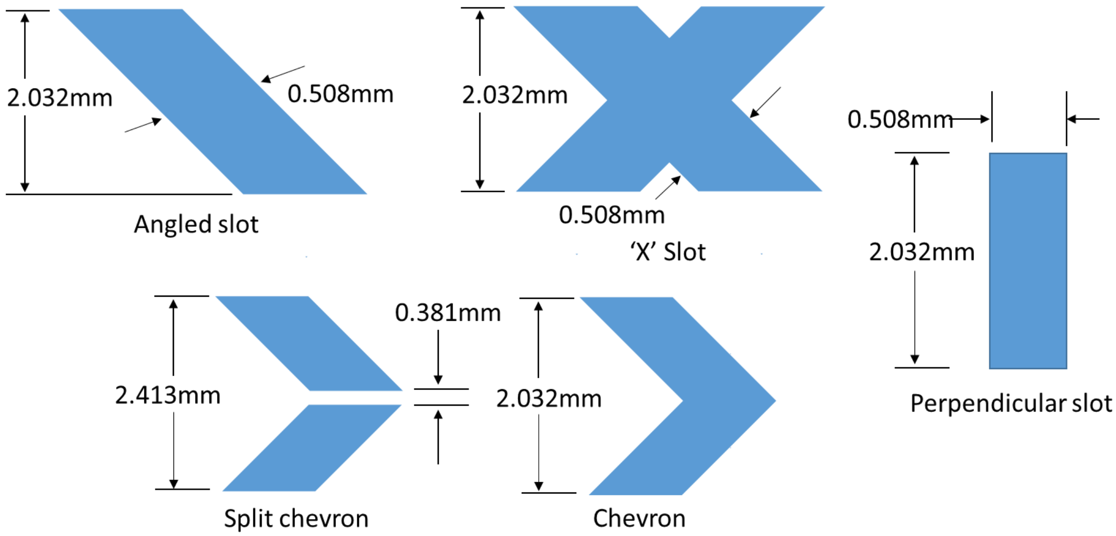

Figure 4. Phase 2 Facesheet perforate geometry.

B. Liner Core Construction

Each facesheet was mounted onto a metallic liner core with a cavity depth of 38.1 mm. The liner core is from a previous investigation that was repurposed for this experiment. To allow for rapid changes of liner configuration, the facesheets are not bonded to the core structure but clamped by their long edges as part of installation in the test rig. Note that the core is constructed for the full length of the GFIT test window (614.4 mm) while the facesheets are only 460.8 mm long. An aluminum blanking plate was fabricated to cover the remaining portion of the core. Figure 5. Liner sample facesheet and filler blank overlaid on core cavity with internal honeycomb. shows a typical arrangement with the blanking plate (right) and the facesheet (left) overlaid on the core.

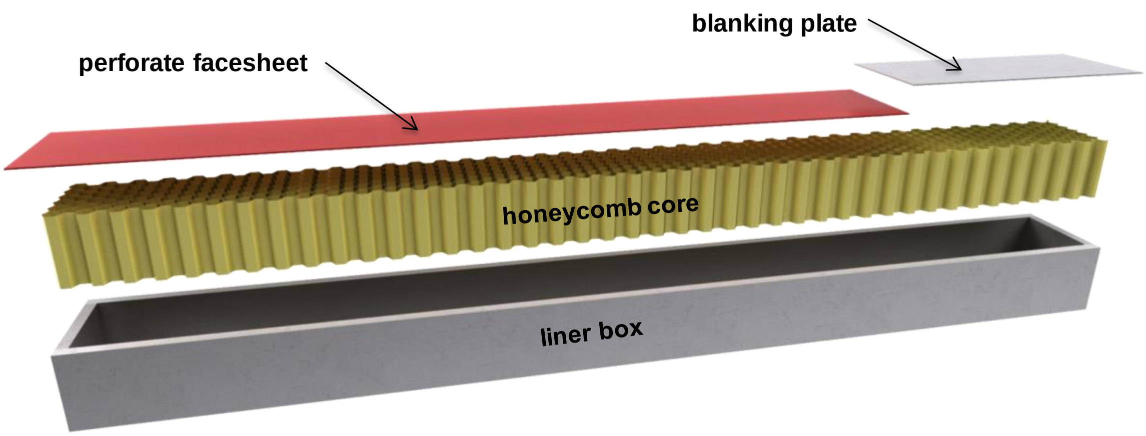

Figure 5. Liner sample facesheet and filler blank overlaid on core cavity with internal honeycomb.

C. Grazing Flow Impedance Tube (GFIT)

The Grazing Flow Impedance Tube (GFIT) is a unique facility originally constructed to determine the acoustic characteristics of noise reduction treatments (acoustic liners) for aircraft jet engine nacelles and nozzles. The facility is a small wind tunnel with a 50.8 mm by 63.5 mm rectangular cross section. The flow path (Figure 6) is a straight duct with a 12-driver upstream acoustic source section, interchangeable lengths of blank duct, a test section holding the liner sample along the upper wall of the duct and an array of 95 measurement microphones leading to a 6-driver downstream source section and anechoic terminating diffuser. Pressurized, heated air is supplied to the entrance of the GFIT while a vacuum system is used at the duct exit to 'pull' the flow out of the tube. This arrangement allows for the static pressure at the test section to be near ambient at all flow velocities while also creating an adiabatic wall condition. In its current configuration, samples can be tested at grazing flow velocities from 0 to Mach 0.6 and sound pressure levels up to 150 dB for the frequency range between 400 and 3000 Hz. At the test section, the wall boundary layers are fully turbulent with flow velocity profiles approaching a fully developed condition.

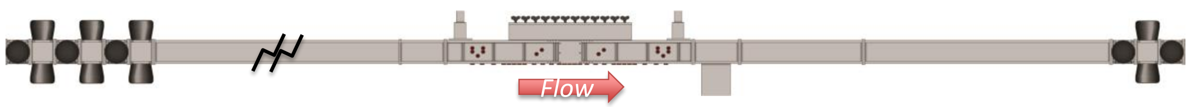

Figure 6. Sketch of the NASA Langley Grazing Flow Impedance Tube (GFIT).

This investigation also makes use of an array of 80 static pressure ports located along the lower wall of the duct to measure the axial pressure distribution. Pressures from these ports are simultaneously sampled by a series of transducers with a +/- 17 kPa range and 0.05% of full-scale accuracy with a fixed sample rate of 100 Hz. A plot of the axial pressure distribution in the test section for the hardwall case is shown in Figure 7. Two ports, one located near the entrance and the other located near the exit of the test section (separated axially by 1.07 m) are also connected to a high-accuracy, differential pressure gauge to measure the static pressure drop between these two locations. This gauge samples at a much slower rate (~10 Hz) but with its smaller 0-6900 Pa range and 0.01% FS accuracy, measurement uncertainty is reduced by a factor of 12.5. A sketch of the test section is included above the plot showing the relative location of the liner and the ports used to compute the static pressure drop (Δp).

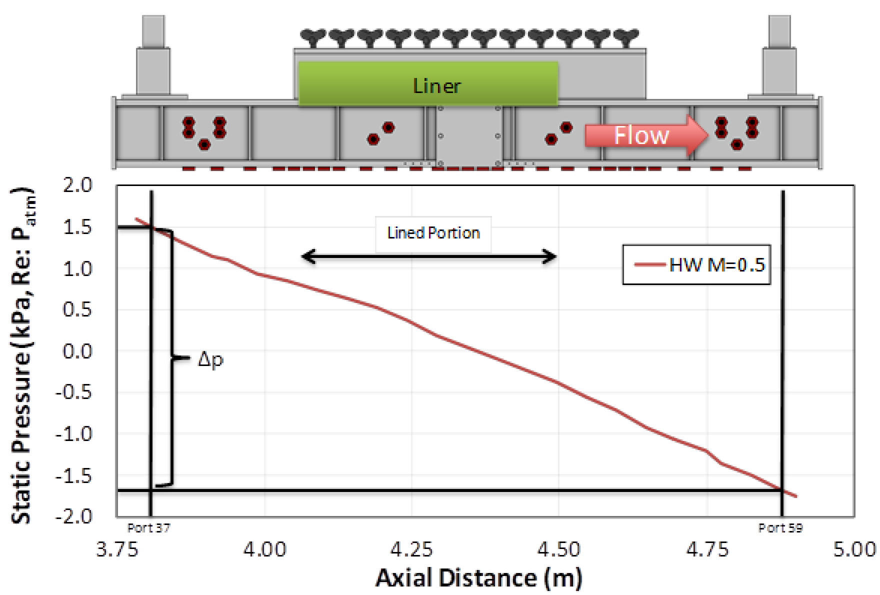

Figure 7. GFIT Test Section Static Pressure Distribution, Hardwall Sample, M=0.5

D. Measurement Process

Following the method set forth by Howerton and Jones [4], averaged static pressure measurements were made for each configuration with no acoustic excitation at M=0.3 and 0.5. For each data set, 1000 readings from each static port were made over a nominal 40 sec period then averaged to give one measurement per port. Simultaneously, similar data were acquired from the high-accuracy gauge to provide the static pressure drop across the length of the liner. For all cases, the target Mach number was held to a tolerance of +/- 0.002 while test section static pressure was adjusted to within +/-130 Pa of atmospheric pressure. Tunnel conditions, including average Mach number and static pressure, were also recorded to allow computation of λ from Equ. (1). Use of a non-dimensional coefficient like λ provides a benefit by normalizing the static pressure data. This normalization reduces the variability of the results, allowing comparison of data from different flow runs where static pressure and Mach number differences (albeit small) can affect the raw Δp measurements. An example of this variation is shown in Figure 8a with a graph of Δp measurements from the smooth wall case at nominally M=0.5. A relationship between Mach number and Δp is readily apparent. Computation of λ from this data results in the plots shown in Figure 8b.

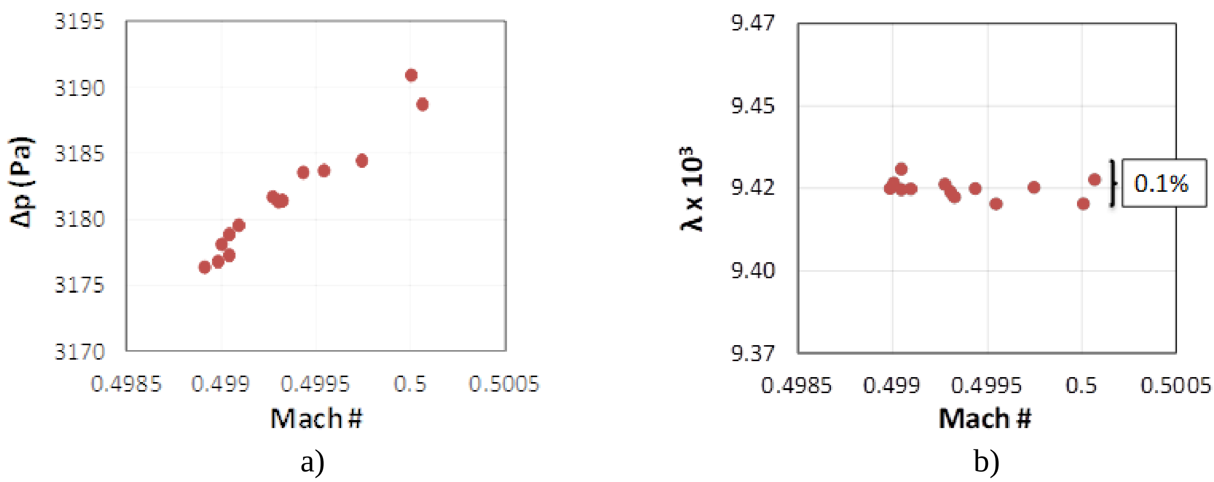

Figure 8. Liner Δp measurements and corresponding values of λ, Smooth wall sample, M=0.5.

The calculated values of λ are independent of the small Mach number changes and variability of the results about the mean is nominally 0.1%, indicating excellent repeatability for back-to-back measurements. Comparisons with other flow speeds show variability decreasing with increasing Mach number, since Δp increases while the accuracy of the pressure gauge is fixed as a percentage of its range. Note that values of λ derived from GFIT pressure measurements cannot be directly related to values of Darcy's friction factor commonly found on a Moody chart. Only a portion of the duct surface is lined and, depending upon M and the axial location of the test section, the flow may not be fully developed.

If one assumes that the contribution of each portion of the duct to the measured value of lambda is proportional to its surface area, the resistance factor of the lined portion can be determined using the following relation:

$$\lambda_{L+SW} = \frac{P - W_L}{P}\lambda_{SW} + \frac{W_L}{P}\left(\frac{S - LL}{S}\lambda_{SW} + \frac{LL}{S}\lambda_L\right) \quad (4)$$

Solving for λ_L gives:

$$\lambda_L = \frac{\frac{P\lambda_{L+SW} - (P - W_L)\lambda_{SW}}{W_L} - (\frac{S - LL}{S})\lambda_{SW}}{\frac{LL}{S}} \tag{5}$$

Tonal acoustic excitation was additionally used for M=0.3 and M=0.5 for frequencies between 400 and 2800 Hz (200 Hz increments) at a *target* sound pressure level (SPL) of 140 and 150 dB (re: 20 μPa). It is important to note that, for certain combinations of frequency and Mach number, the higher SPL was not achieved but was usually at least 6 dB greater than the lower target. Static pressure measurements were performed simultaneously with the acoustic surveys to evaluate the effect of acoustic excitation on liner drag. Acoustic measurements were performed to allow for comparison of liner impedances educed using the Straightforward Method of Watson [7].

IV. RESULTS AND DISCUSSION

A. Static Pressure Measurements

Figure 9 shows the liner resistance factor, λ_L, computed from Equation (5) for the eleven facesheet and two smooth wall configurations from Phase 1 tested at Mach numbers of 0.3 and 0.5 with no sound.

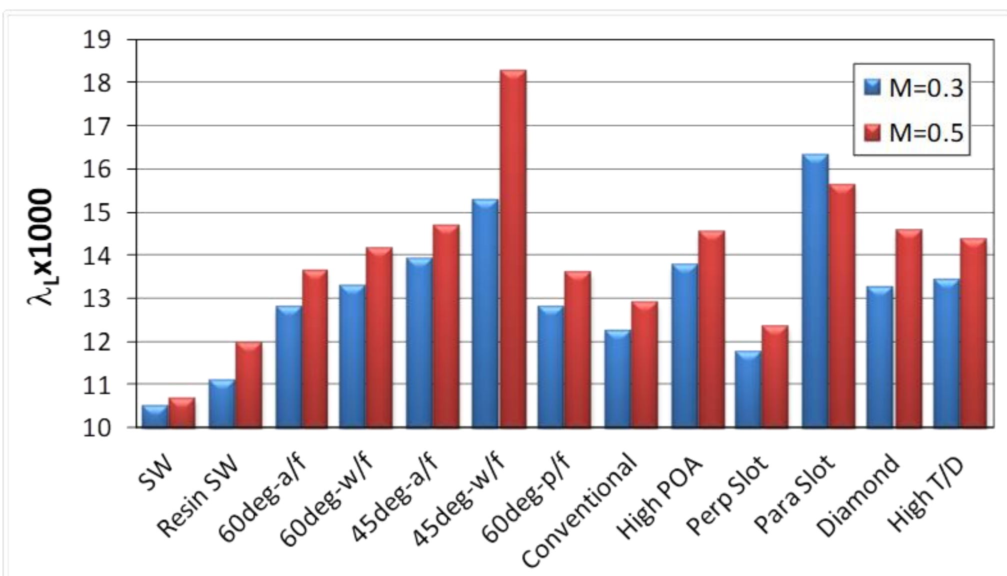

Figure 9. Liner resistance factor (λ_L) x 1000 for M=0.3 and 0.5, no sound.

Generally, λ_L increases with increasing Mach number except for the Parallel Slot configuration which saw a slight decrease. All configurations produce a drag penalty relative to the Resin SW. Angling the perforations against the flow (a/f cases) proved very detrimental to liner drag, especially for the shallower 45 deg configuration. Overall, many of the configurations tested result in increased drag relative to the Conventional perforate design. Only the Perpendicular Slot shows a reduction but still carries a penalty relative to both smooth wall configurations. The Resin SW result is also higher than the aluminum SW for both Mach numbers indicating increased surface roughness for the printed sample.

Figure 10 is a plot of the percent difference of the liner resistance factor (λ_L) relative to the Resin SW configuration. None of the angled, round hole designs perform better than the straight-hole Conventional configuration. Of those, facesheets with perforations oriented with the flow (w/f cases) are measurably worse than their counterparts with perforations oriented against or perpendicular the flow (p/f case). Note that for the 45 deg angle, the penalty more than doubled for M=0.5. The High T/D design produces a 20% increase that was nearly double the result for the Conventional configuration. This result seems to contradict the findings of Hwang, but one should note the diameter of those perforations were an order of magnitude smaller than what was tested here. As noted earlier, smaller perforations have been shown to reduce drag for a given porosity. Of all the alternate configurations tested, only the Perpendicular Slot design performs better than the Conventional with a $\Delta\lambda_L$ approximately 50% lower and penalty relative to the Resin SW of ~5%. The High POA and Parallel Slot cases show penalties of over 20% and 30%, respectively, indicating that small changes in the perforate configuration can have a large impact on λ_L.

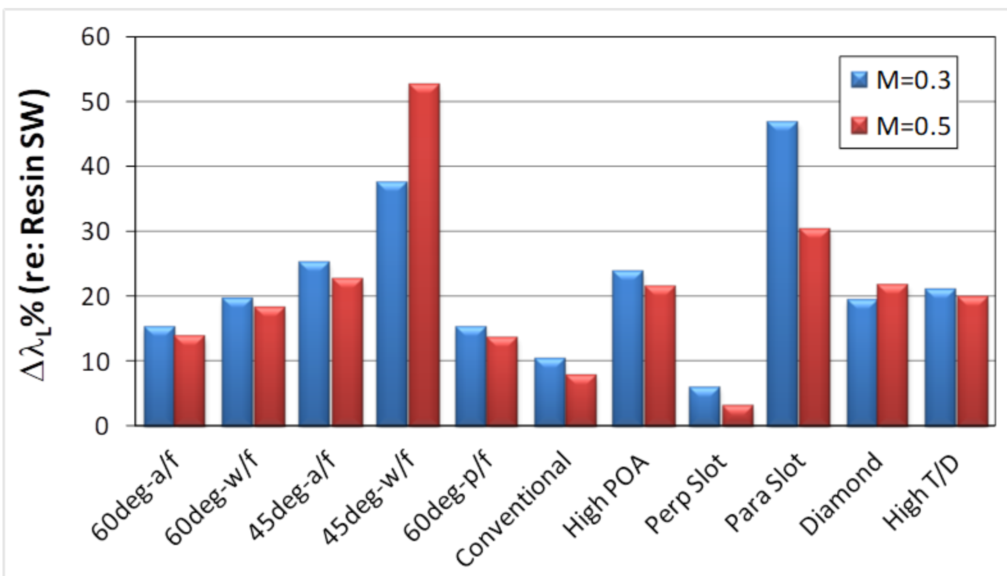

Figure 10. Percent difference in λ_L (relative to Resin SW) for M=0.3 and 0.5, no sound.

Similar results for the Phase 2 samples are shown in Figure 11 at M=0.5. For these slot-derived designs, again, the Perpendicular Slot provides the lowest measured resistance factor. However, the error bars show a total measurement uncertainty of +/- 2%, which renders the observed differences between configurations statistically insignificant. A reduction of measurement uncertainty is necessary to continue the evaluation of low-drag facesheet perforates to achieve the goal of a 60% penalty reduction.

Two improvements to the drag measurement process are planned that should reduce uncertainty significantly. The first involves moving the GFIT static ports used in the measurement process closer together. This will increase the ratio of lined vs. unlined duct wall area by reducing

S in Eq. 5 making the calculation of λ_L less sensitive to variations in the measurement of λ_{L+SW}. The second improvement is the incorporation of new pressure transducers better tailored to the Δp created by a liner at each Mach number. As the accuracy of these transducers is a function of their full-scale range, matching their range to the static pressure drop being measured will improve overall accuracy. This is especially true for the lower Mach numbers where the measured pressures were nearly an order of magnitude less than the transducer range for the current study.

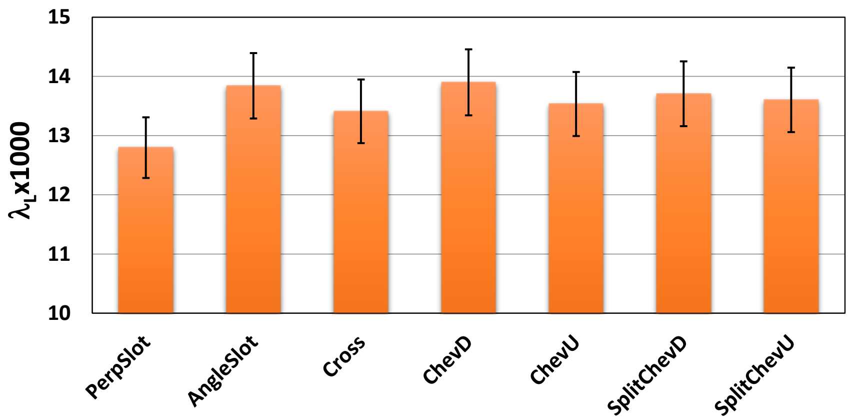

Figure 11. Liner resistance factor (λ_L) x 1000 for M=0.5, no sound.

B. Effects of Acoustic Excitation on Drag

Each liner configuration was evaluated in the presence of acoustic tonal excitation at a target total SPL of 140 and 150 dB. For Phase 1, frequencies ranged from 400 Hz to 3000 Hz, in 200 Hz increments. It was postulated prior to the test that the oscillatory motion of fluid through the facesheet perforations would affect the measured resistance factor. Significant variation in λ_L at or near the frequencies of resonance (~1700 Hz for these configurations) and anti-resonance were also postulated. Figure 12 shows resistance factor spectra for the two Mach numbers and SPL's. From these plots, several trends emerge. The resistance factor of the liner varies slightly with frequency. The variation increases with increasing SPL and decreases with increasing Mach number. Thus, there exist combinations of Mach number and SPL for which λ_L is relatively invariant with frequency. This behavior is desired from a design perspective since it can eliminate frequency as an optimization variable. For flow speeds of Mach 0.5, even the 150 dB level results in variations only on the order of 10%, significantly less than that observed for the Mach 0.3 cases. The expectation of some discernable effect of resonance is not borne out by the data for any Mach number or SPL. In fact, the most notable feature of the spectra is the dip in the 150 dB results at 1200 Hz. The current design of the GFIT acoustic speaker array and anechoic terminations seems to inhibit efficient acoustic energy transmission from the loudspeakers into the duct at that frequency, limiting the maximum SPL at that frequency to approximately 141 dB. This level is substantially less than the other frequencies tested which produces less of an effect on the liner resistance factor due to reduced jetting of vortices though the perforations.

Phase 2 results are given in Figure 13 for flow at M=0.5 and 150 dB acoustic excitation. The observed trends are similar to the no sound results with the Perpendicular Slot perforate generally producing the lowest λ_L values. It is interesting to note that, while the Angle Slot and Chevron D configurations had similar resistance factors for no sound, the Angle Slot generally higher drag when excited acoustically.

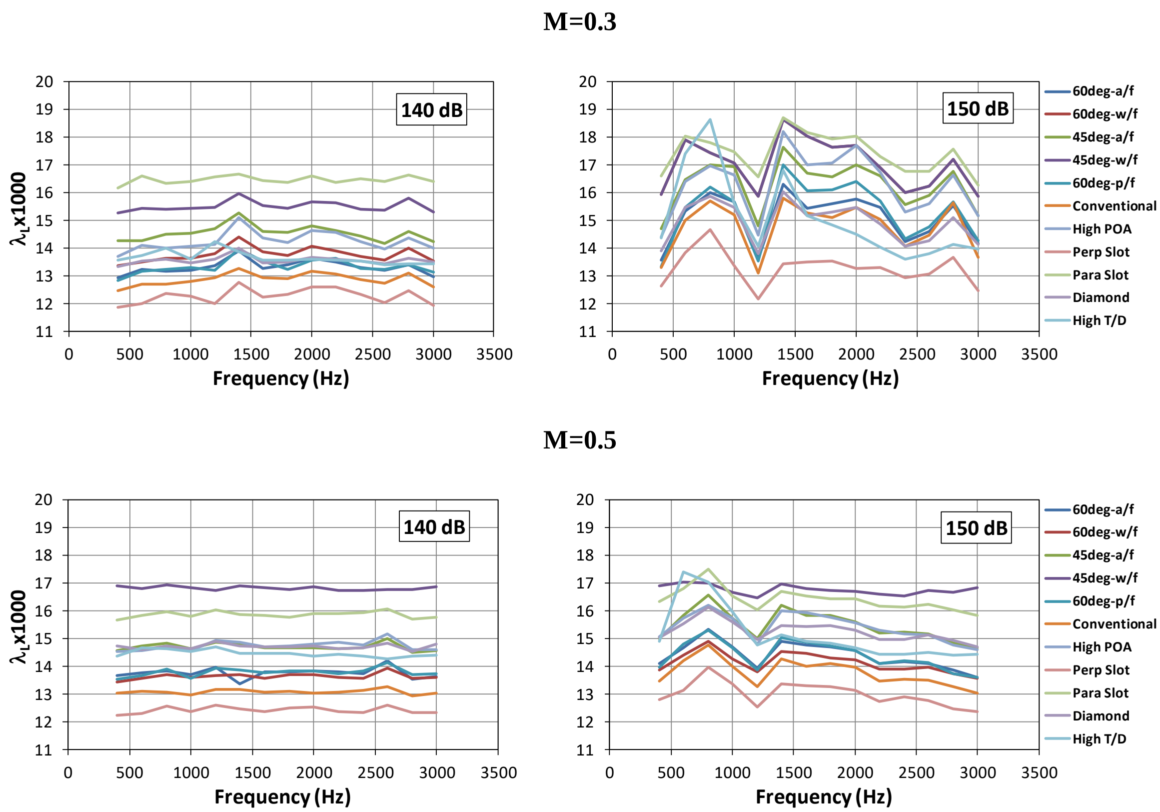

Figure 12. Variation of resistance factor with acoustic excitation (Phase 1).

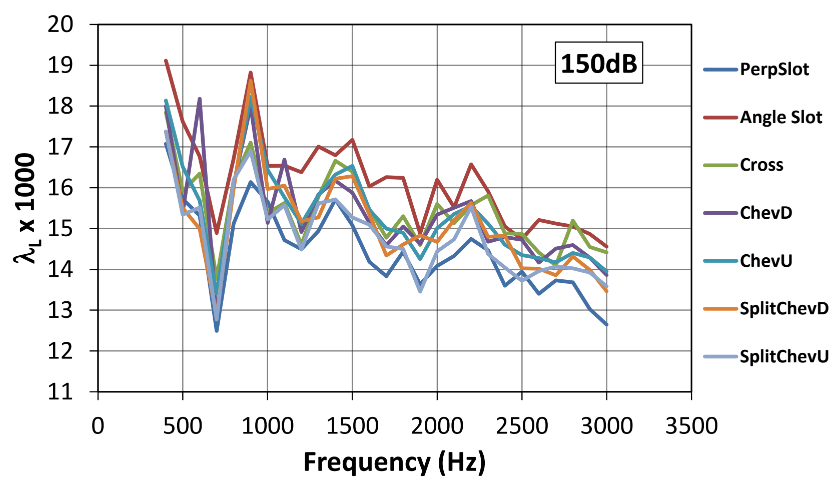

Figure 13. Variation of resistance factor with acoustic excitation, M=0.5 (Phase 2).

C. Acoustic Measurements

For each Phase 1 liner configuration, full acoustic pressure profiles were acquired at M=0.3 and 0.5 for impedance eduction and evaluation of attenuation. As noted before, there are certain frequencies at M=0.5 where 150 dB was not achieved. For that reason, the acoustic results presented below are for the M=0.5, 140 dB cases. These educed impedance spectra are compared to determine if variations in perforate geometry and orientation have significant impact on the liner acoustic performance relative to the Conventional configuration. Ideally, variations in perforate shape would have minimal acoustic effect [8], thereby allowing for selection based on drag performance. Results from the High T/D sample are omitted for the sake of clarity since that configuration's significantly higher resistance values, relative to the other facesheets, would expand the scale and obscure details of the other spectra.

Figure 14 shows the normalized impedance spectra (all impedances are normalized by ρc) for each configuration. For resistance, the differences between facesheets are less than ~0.7 at all frequencies and variation in reactance is generally less than 0.5. Resonance for these configurations varies between approximately 1700 and 2000 Hz with the majority clustered near 2000 Hz. The Perpendicular Slot and Diamond liners exhibit a lower resonance near 1700 Hz. The shapes of the impedance spectra for all of the liners are similar (note the expanded scale for the resistance spectra). These results imply that a low-drag design could be tailored to closely match the impedance spectra of a higher-drag, conventional design. Figure 15 contains impedance spectra for the Conventional and low-drag Perpendicular Slot configurations. The educed resistance and reactance spectra compare favorably and imply that acoustic performance does not have to be sacrificed in order to reduce liner drag.

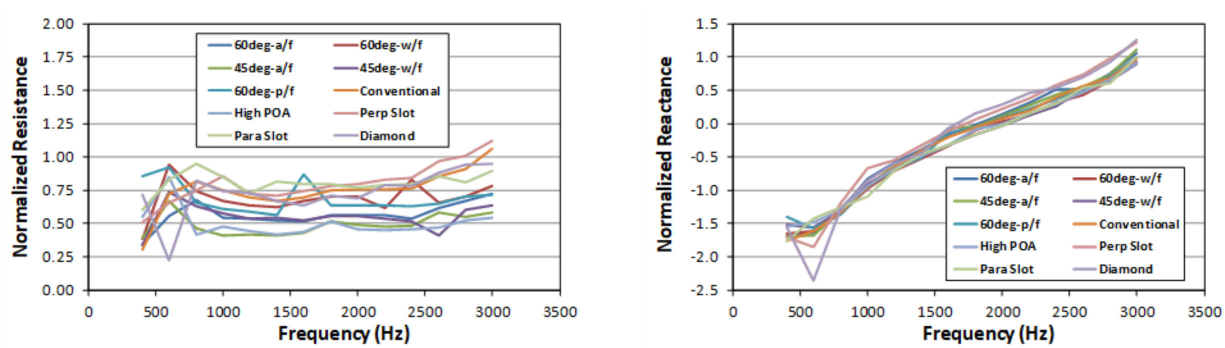

Figure 14. Normalized impedance spectra for each Phase 1 configuration, M=0.5, 140 dB.

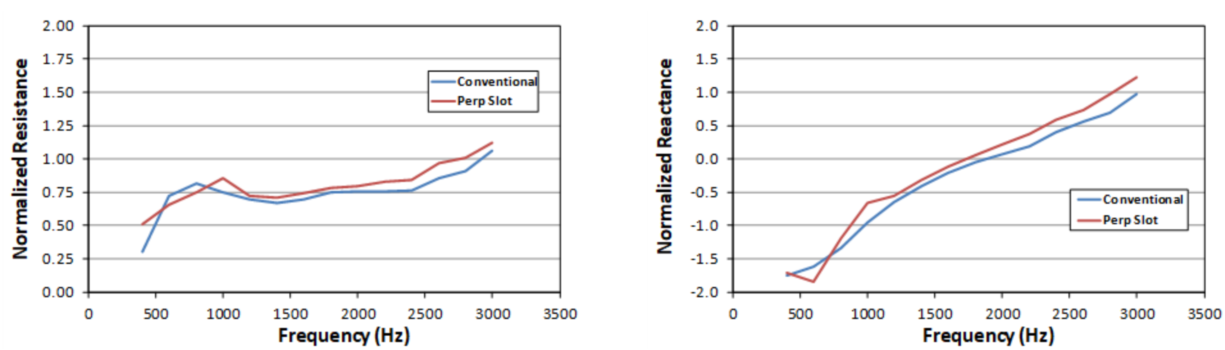

Figure 15. Comparison of normalized impedance spectra, Conventional (round hole) vs. Perpendicular Slot configurations, M=0.5, 140 dB.

This conclusion is further supported by the data shown in Figure 16 where the acoustic pressure profiles are plotted for the Conventional and Perpendicular Slot at selected frequencies bracketing resonance. X=0 corresponds to a point 203.2 mm upstream of the liner leading edge. The profiles for each frequency compare favorably.

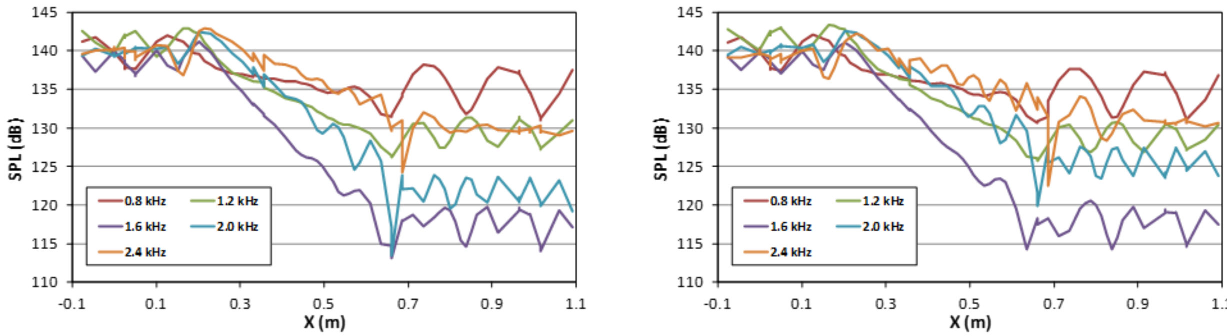

a) Conventional b) Perpendicular Slot

Figure 16. Comparison of axial attenuation, M=0.5, 140 dB.

Another method of evaluating liner performance is to compare the levels of attenuation achieved by the various configurations. This calculation gives a gross estimate of the effect these variations in perforate geometry have on the overall acoustic performance of the liner. For this study, a simple estimate of attenuation was calculated using the difference in sound pressure levels measured at the leading and trailing edges of the duct (203.2 mm upstream of liner leading edge and 355.6 mm downstream of liner trailing edge, respectively). Such a result does include the effects of reflections from these edges and the influence of the duct termination. However, it still provides a useful quantity for comparison. Figure 17 shows the results of this calculation and confirms that for much of the frequency range tested, the differences in perforate geometry do not significantly impact the resulting liner attenuation.

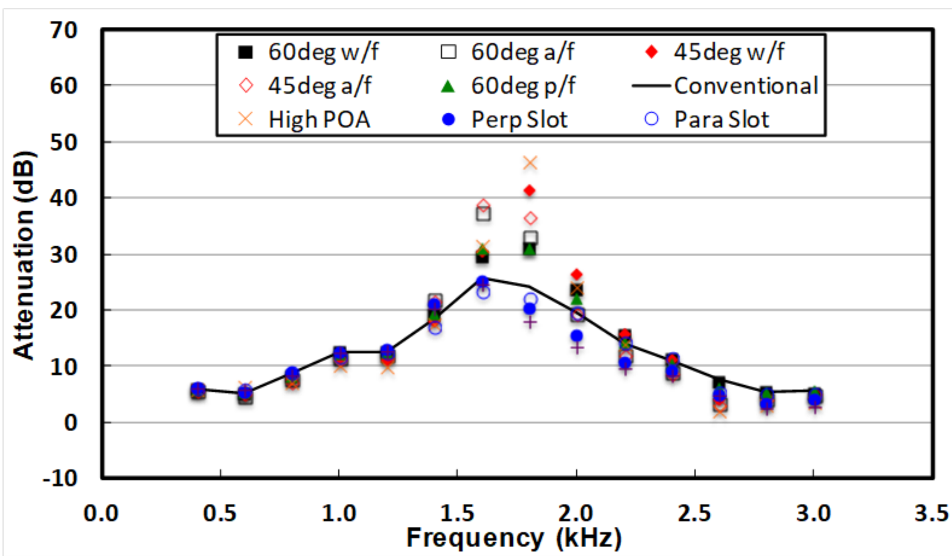

Figure 17. Comparison of overall liner attenuation, M=0.5, 140 dB.

For frequencies near resonance (approximately 1900 Hz for this liner geometry), the variation between configurations grows to as much as +20/-5dB relative to the Conventional perforate. Figure 18 presents the average difference in attenuation (in dB), relative to the Conventional configuration. Using this metric, it can be shown that the Perpendicular Slot, Parallel Slot and Diamond perforates perform slightly worse overall than the Conventional configuration. Several perforates have average attenuations better than the Conventional configuration, but all the variation is within +/- 1.5 dB indicating that the change in perforate geometry has little effect on overall liner performance.

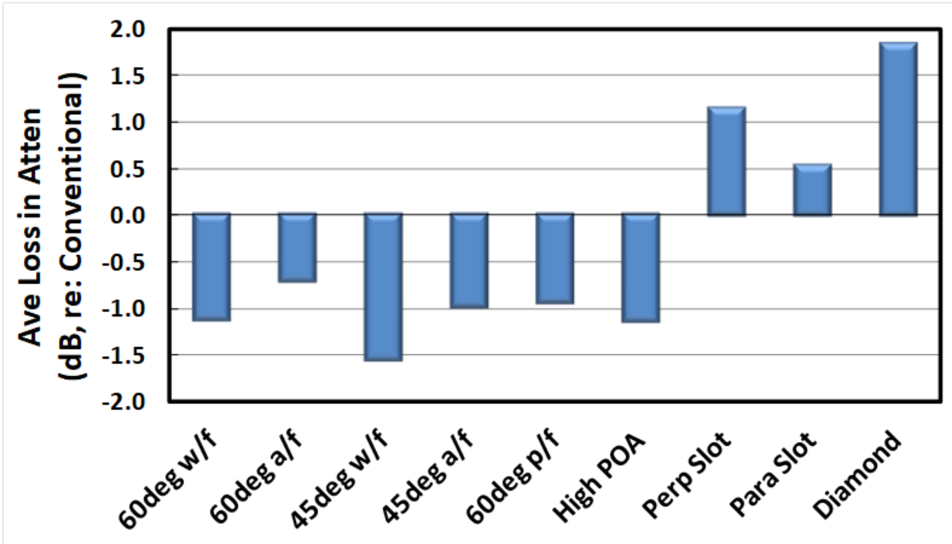

Figure 18. Relative attenuation loss, M=0.5, 140 dB.

Similar calculations for the Phase 2 configurations were not performed since those configurations did not offer any drag improvements over the Perpendicular Slot configuration identified in Phase 1.

V. CONCLUDING REMARKS

A set of liner facesheets was tested in the NASA Langley GFIT to assess their drag relative to a smooth wall and a conventional straight, round-hole perforate. Several observations were made:

1. Adding angle/skew to a conventional, round-hole perforate configuration increased facesheet drag, especially for holes angled at 45 deg.

2. Angling the holes with the flow increased the measured resistance factors more than angling against the flow. The shallower 45 deg case with this orientation produced the most drag of all configurations tested.

3. The Phase 1 Perpendicular Slot configuration produced the lowest drag and was the only perforate design that performed better than the Conventional design.

4. The slot-based Phase 2 configurations produced resistance factors marginally higher than the Perpendicular Slot but the differences were not statistically significant given the uncertainty in the measurement.

5. Changes to the perforate geometry caused variation to the normalized resistance spectra, on the order of 0.5.

6. Changes to perforate geometry caused minimal variation to the normalized reactance spectra. Resonant frequencies clustered around 2000 Hz for most cases. The Diamond and Perpendicular Slot liners resonated near 1700 Hz.

7. Compared to the Conventional configuration, differences in overall attenuation between the perforate geometries were small.

8. Acoustic liner performance need not be sacrificed to reduce liner drag. The acoustic characteristics of the identified low-drag perforate were sufficiently close to the conventional design that only minor geometry changes would be required to recover any lost acoustic performance.

9. Further work to reduce liner drag measurement uncertainty should be performed before evaluating additional low-drag concepts in order to make the comparisons statistically meaningful.

References

[1] C. K. Tam, N. N. Pastouchenko, M. G. Jones and W. R. Watson, "Experimental Validation of Numerical Simulations for an Acoustic Liner in Grazing Flow," *AIAA Paper 2013-2222, 19th AIAA/CEAS Aeroacoustics Conference,* May 2013.

[2] M. K. Drouin, J. M. Gallman and R. F. Olsen, "Sound Level Effect on Perforated Panel Boundary Layer Growth," *AIAA Paper 2006-2411*, *12th AIAA/CEAS Aeroacoustics Conference*, May 2006.

[3] R. H. Thomas, C. L. Burley, L. V. Lopes, C. J. Bahr, F. H. Gern and D. E. Van Zante, "System Noise Assessment and the Potential for a Low Noise Hybrid Wing Body Aircraft with Open Rotor Propulsion," *AIAA Paper 2014-0258, 52nd Aerospace Sciences Meeting*, January 2014.

[4] B. M. Howerton and M. G. Jones, "Acoustic Liner Drag: A Parameteric Study of Conventional Configurations," *AIAA Paper 2015-2230, 21st AIAA/CEAS Aeroacoustics Conference,* June 2015.

[5] J. Nikuradse, "Laws of Flow in Rough Pipes," NACA TM-1292, November 1950.

[6] D. P. Hwang, "A Proof of Concept Experiment for Reducing Skin Friction by Using Micro-Blowing Technique," *AIAA Paper 97-0546, 35th Aerospace Sciences Meeting and Exhibit,* January 1997.

[7] W. R. Watson and M. G. Jones, "A Comparative Study of Four Impedance Eduction Methodologies Using Several Test Liners," *AIAA Paper 2013-2274*, *19th AIAA/CEAS Aeroacoustics Conference*, May 2013.

[8] K. K. Ahuja and R. J. Gaeta, "Active Control of Liner Impedance by Varying Perforate Orifice Geometry," *NASA CR-2000-210633*, December 2000.

Acknowledgements

The authors would like to thank Carol Harrison of the NASA Langley Structural Acoustics Branch, Martha Brown of the Aeroacoustics Branch and Alonso Reid of Science and Technology Corporation for their efforts in collecting the experimental data. Funding for this effort was provided under NASA's Advanced Air Transport Technology Project for the Advanced Air Vehicles Program.